Menemui Matematik (Discovering Mathematics)
Vol. 45, No. 2: 185 - 199 (2023)

Nanofluid flow between disks in the presence of thermal radiation and heat source: Stability analysis

Rusya Iryanti Yahaya[1], Aniza Abd Ghani[2], Norihan Md Arifin[1,2], Fadzilah Md Ali[1,2] and Siti Suzilliana Putri Mohamed Isa[1,3]

[1]*Institute for Mathematical Research, Universiti Putra Malaysia, 43400 UPM Serdang, Selangor*
[2] *Department of Mathematics and Statistics, Universiti Putra Malaysia, 43400 UPM Serdang, Selangor*
[3]*Centre of Foundation Studies for Agricultural Science, Universiti Putra Malaysia, 43400 UPM Serdang, Selangor*
[1]rusyairyanti@gmail.com

ABSTRACT

The internal flow between disks is used in various applications, including rotating machinery, air-cleaning machines, food processing technology, and gas turbine rotors. The present study analyses the nanofluid flow between a non-permeable, stationary disk and a permeable, rotating, shrinking disk. Radiation and heat generation effects are included in the proposed governing partial differential equations and boundary conditions. Then, non-linear ordinary differential equations and boundary conditions are derived through the similarity transformations for numerical computation in MATLAB. Dual solutions from the computation prompted a stability analysis; only the first solution is stable. Enhancing thermal radiation and heat generation parameters reduces and increases the temperature profile throughout the internal flow. Meanwhile, increasing the shrinking parameter and Reynolds number reduces the radial and tangential velocities in some regions close to the stationary, non-permeable disk.

Keywords: Disk, Dual solutions, Nanofluid, Stability analysis, Thermal radiation, Heat source

INTRODUCTION

Cooling-air systems such as gas turbine rotors usually involve fluid flow over more than one disk. The disk may rotate in close proximity to a stationary casing or near another disk that is either co-rotating or, less frequently, contra-rotating (Kilic and Owen, 2003). Due to various applications of flows between disks, researchers have actively conducted studies with different working fluids, physical conditions, and controlling parameters. One of the earliest studies on the fluid flow between disks was conducted by Rajagopal (1992). This study considered viscous and viscoelastic fluids, and the flow problem was solved for symmetric and asymmetric solutions. Soong (2003) and Kilic and Owen (2003) then examined the flow between two disks rotating independently and with different speeds, respectively. Then, Khan and Mahmood (2016) discussed the magnetohydrodynamics (MHD) flow of Oldroyd B-nanofluid between infinite stretching disks. The MHD nanofluid flow between stationary and rotating disks was then analysed by Upadhya et al. (2021). Bilal et al. (2022) then extended this study with chemical reactions. The broad applicability of flow between disks has prompted various other research (see Awati et al. (2018), Weghal and Ashraf (2020), Ahmadian et al. (2020), Habu et al. (2022), Usman et al. (2022), Hussain and Xu (2022), Jalili et al. (2023), Khan et al. (2023), Ghasemi and Gouran (2023), and Umavathi et al. (2023)). Recently, Yahaya et al. (2023) discussed the nanofluid flow between a non-permeable, stationary disk and a permeable, rotating disk in the presence of thermal radiation and heat generation. In this study, dual solutions were found when considering the shrinking case, and the highest heat transfer rate was produced by Mn-$ZnFe_2O_4/C_2H_6O_2$ nanofluid.

Numerical computation of a boundary value problem may result in a unique solution, no solution, or multiple solutions. For example, Zulkifli and Md Ali (2023) discovered dual solutions when considering the flow of nanofluid over a permeable shrinking sheet. A stability analysis can

be conducted to identify the physically meaningful solution among the obtained multiple solutions. Merkin (1986) showed the stability analysis on dual solutions, which helps determine the realizability of the solutions in real applications. This study was then referred to and followed by other researchers, such as Zainal et al. (2021), Lanjwani et al. (2023), and Duguma et al. (2023), when dealing with multiple solutions. In these studies, only one solution was found to be stable and physically meaningful. The stable solution was noted to have an initial decay of disturbance, while the unstable solution contained an initial growth of disturbance.

In the current investigation, the flow problem by Yahaya et al. (2023) will be extended with a comprehensive study on the effects of thermal radiation and heat generation on the nanofluid flow. The boundary conditions and partial differential equations that control the flow problem will be simplified and numerically solved in MATLAB. Then, stability analysis will be carried out to identify the stable and significant solution for the present study.

MATHEMATICAL FORMULATION

Figure 1 illustrates the physical model of the steady flow problem. A nanofluid is considered to flow between a stationary, non-permeable disk (lower disk) and a permeable, rotating, shrinking disk (upper disk) separated by a distance l. Here, the distance l is assumed to be very small compared to the radii of the disks (Ahmadian et al., 2020). (r, φ, z) are cylindrical coordinates with $r-$ axis measured in the vertical direction and $z-$ axis measured in the horizontal direction. The rotating upper disk has a velocity of $\Omega\,\varepsilon$ with Ω as the angular velocity. Meanwhile, ε $(0 < \varepsilon \leq 1)$ is a regulator which controls the rotation of the disk with $\varepsilon > 0$ for rotation and $\varepsilon = 0$ for a stationary disk. Then, the nanofluid is composed of water (H_2O) and ethylene glycol ($C_2H_6O_2$) suspended by cobalt ferrite ($CoFe_2O_4$) and Mn-Zn ferrite ($Mn\text{-}ZnFe_2O_4$) nanoparticles. The nanofluid temperature is given by T, while the temperature of the lower and upper disks is T_1 and T_2, respectively.

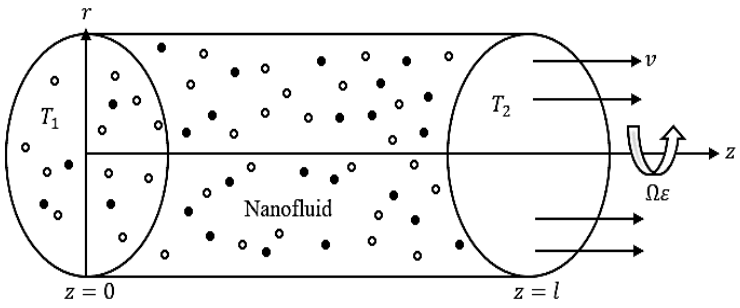

Figure 1. Physical model of the flow problem.

Governing equations and boundary conditions

The governing boundary layer equations for the flow problem can be expressed as (Upadhya et al., 2021):

$$\frac{1}{r}\frac{\partial\,(r\,u)}{\partial\,r} + \frac{\partial\,w}{\partial\,z} = 0, \tag{1}$$

$$u\,\frac{\partial\,u}{\partial\,r} + w\,\frac{\partial\,u}{\partial\,z} = -\frac{1}{\rho_n}\,\frac{\partial\,p}{\partial\,r} + \frac{\mu_n}{\rho_n}\left[\left(\frac{\partial}{\partial\,r}\left(\frac{u}{r}\right)\right) + \frac{\partial^2 u}{\partial\,z^2}\right] + \frac{v^2}{r}, \tag{2}$$

$$\frac{u}{r}\,\frac{\partial\,(r\,v)}{\partial\,r} + w\,\frac{\partial\,v}{\partial\,z} = \frac{\mu_n}{\rho_n}\left[\frac{\partial^2 v}{\partial\,z^2} + \left(\frac{\partial}{\partial\,r}\left(\frac{v}{r}\right)\right)\right], \tag{3}$$

$$u\,\frac{\partial\, w}{\partial\, r}+w\,\frac{\partial\, w}{\partial\, z}=\frac{\mu_n}{\rho_n}\left[\frac{1}{r}\,\frac{\partial\, w}{\partial\, r}+\frac{\partial^2 w}{\partial\, z^2}\right]-\frac{1}{\rho_n}\,\frac{\partial\, p}{\partial\, z}, \tag{4}$$

$$u\,\frac{\partial\, T}{\partial\, r}+w\,\frac{\partial\, T}{\partial\, z}=\frac{Q_0}{\left(\rho\, C_p\right)_n}\,(T-\,T_2)-\frac{1}{\left(\rho\, C_p\right)_n}\frac{\partial\, q_r}{\partial\, z}+\frac{k_n}{\left(\rho\, C_p\right)_n}\left[\frac{1}{r}\,\frac{\partial\, T}{\partial\, r}+\frac{\partial^2 T}{\partial\, z^2}\right], \tag{5}$$

with thermal radiation and internal heating considered in the energy equation (5). The boundary conditions are:

$$u(r,0)=0,\qquad v(r,0)=0,\qquad w(r,0)=0,\qquad T(r,0)=\,T_1\quad\text{at}\quad z=0, \tag{6}$$

$$u(r,l)=0,\qquad v(r,l)=r\,\Omega\,\lambda,\qquad \mathrm{w}(r,l)=\,\varepsilon\,w_0,\qquad T(r,l)=\,T_2\ \text{at}\ \ z=l. \tag{7}$$

In the above equations, $u, v,$ and w are the velocity components along the $r, \varphi, z-$axes. Meanwhile, w_0 is the constant mass flux velocity with $w_0 > 0$ for suction and $w_0 < 0$ for injection, p is the pressure, Q_0 is the heat generation/absorption coefficient, q_r is the radiation heat flux, and $\lambda(< 0)$ is the shrinking parameter.

Correlations and thermophysical properties of nanofluid

The correlations and thermophysical properties of the nanofluid are given in equation (8) and Table 1, respectively:

$$\left.\begin{aligned}\frac{\mu_n}{\mu_f}&=\frac{1}{(1\,-\,\phi)^{2.5}},\\ \rho_n&=(1-\phi)\,\rho_f+\,\phi\,\rho_s,\\ \frac{k_n}{k_f}&=\frac{k_s\,+2\,k_f\,-2\,\phi\,(k_f\,-\,k_s)}{k_s\,+2\,k_f\,+\,2\,\phi\,(k_f\,-\,k_s)},\\ \left(\rho C_p\right)_n&=(1-\,\phi)\left(\rho\,C_p\right)_f+\,\phi\left(\rho\,C_p\right)_s.\end{aligned}\right\}. \tag{8}$$

Table 1. Thermophysical properties of water, ethylene glycol, $CoFe_2O_4$, and $Mn\text{-}ZnFe_2O_4$ nanoparticles (Ahmed et al., 2019)

Properties	Water	Ethylene glycol	$CoFe_2O_4$	$Mn\text{-}ZnFe_2O_4$
Thermal conductivity, $\boldsymbol{k}$ [W/m K]	0.613	0.349	3.7	5
Heat capacity, $\boldsymbol{C_p}$ [J/kg K]	4 179	2 382	700	800
Density, $\boldsymbol{\rho}$ [kg/m^3]	997.1	1 116.6	4 907	4 900
Prandtl number, $\boldsymbol{Pr}$	6.96	204	-	-

The suffixes n, s, and f represent the nanofluid, nanoparticles, and base fluid, respectively. Further, ϕ is the nanoparticle volume fraction, μ is the dynamic viscosity, ρ is the density, k is the thermal conductivity, and ρC_p is the effective heat capacity with C_p as the heat capacity at constant pressure.

Non-linear ordinary differential equations and boundary conditions

By using the Rosseland approximation and the Taylor series, $T^4 \approx 4T_\infty^3 T - 3T_\infty^4$, and equation (5) can be written as (Bataller, 2008; Ishak, 2010; Magyari and Pantokratoras, 2011):

$$u\,\frac{\partial\, T}{\partial\, r}+w\,\frac{\partial T}{\partial\, z}=\,\frac{1}{\left(\rho\, C_p\right)_n}\left[\left(k_n\left(\frac{1}{r}\left(\frac{\partial\, T}{\partial\, r}\right)+\,\frac{\partial^2 T}{\partial\, z^2}\right)+\frac{16\,\sigma^*\,T_2^3}{3\,k^*}\,\frac{\partial^2 T}{\partial\, z^2}\right)\right]+\frac{Q_0}{\left(\rho\, C_p\right)_n}\,[(T-\,T_2)\theta(\eta)], \tag{9}$$

with q_r as the radiative heat flux, σ^* and k^* denote the constant of Stefan-Boltzmann and the coefficient of mean absorption, respectively.

Then, the following similarity variables are introduced (Upadhya et al., 2021):

$$\left.\begin{aligned} u = r\Omega\, f'(\eta), \quad v = r\,\Omega\, g(\eta), \quad w = -2\,w_0 f(\eta), \quad \theta(\eta) = \frac{T - T_2}{T_1 - T_2}, \\ p = -\frac{1}{2}\rho_f\, r^2\,\Omega^2\, A + \rho_f\, w_0^2\, P(\eta), \quad \eta = \frac{z\,\Omega}{w_0}, \end{aligned}\right\}, \tag{10}$$

where the prime denotes differentiation with respect to η and A is an arbitrary constant.

Next, the pressure term in equations (2) and (4) are eliminated to obtain:

$$\begin{aligned} &\frac{\partial}{\partial z}\left(u\,\frac{\partial u}{\partial r}\right) + \frac{\partial}{\partial z}\left(w\,\frac{\partial u}{\partial z}\right) - \frac{\partial}{\partial r}\left(w\,\frac{\partial w}{\partial z}\right) - \frac{\partial}{\partial z}\left(\frac{v^2}{r}\right) \\ &= \frac{\mu_n}{\rho_n}\left[\frac{\partial}{\partial z}\left(\frac{\partial}{\partial r}\left(\frac{u}{r}\right)\right) + \frac{\partial}{\partial z}\left(\frac{\partial^2 u}{\partial z^2}\right) - \frac{\partial}{\partial r}\left(\frac{\partial^2 w}{\partial z^2}\right)\right], \end{aligned} \tag{11}$$

and after substituting (10) into equations (3), (9), and (11), we obtain the following non-linear ordinary differential equations:

$$f'''' = Re\frac{\rho_n/\rho_f}{\mu_n/\mu_f}(-2\,ff''' - 2gg'), \tag{12}$$

$$g'' = Re\frac{\rho_n/\rho_f}{\mu_n/\mu_f}(2gf' - 2fg'), \tag{13}$$

$$\theta'' = \frac{PrRe}{\left(\frac{k_n}{k_f} + \frac{4}{3}\,Rd\right)}\frac{\left(\rho C_p\right)_n}{\left(\rho C_p\right)_f}\left(-2f\,\theta' - \frac{Q\,\theta}{\left(\rho C_p\right)_n/\left(\rho C_p\right)_f}\right), \tag{14}$$

Here, Pr is the Prandtl number, Re is the Reynolds number, Rd is the radiation parameter, and Q is the heat generation/absorption parameter, given by:

$$Pr = \frac{(\mu C_p)_f}{k_f}, \quad Re = \frac{w_0^2}{\Omega\,\nu_f}, \quad Rd = \frac{4\,\sigma^*\,T_2^3}{k_f\,k^*}, \quad Q = \frac{Q_0}{\Omega\,(\rho C_p)_f},$$

where $\nu = \mu/\rho$ is the kinematic viscosity. The boundary conditions become:

$$\left.\begin{aligned} f(0) = 0, \; f'(0) = 0, \; g(0) = 0, \; \theta(0) = 1, \\ \theta(1) = 0, \; f'(1) = 0, \; g(1) = \lambda, \; f(1) = -\varepsilon/2\,. \end{aligned}\right\}. \tag{15}$$

STABILITY ANALYSIS

Following the previous studies, the dimensionless time variable, $\tau = \Omega t$ with t as time, is introduced into the similarity variables (10) to form:

$$\left.\begin{aligned} u = r\Omega\, f'(\eta,\tau), \quad v = r\,\Omega\, g(\eta,\tau), \quad w = -2\,w_0 f(\eta,\tau), \quad \theta(\eta,\tau) = \frac{T - T_2}{T_1 - T_2}, \\ p = -\frac{1}{2}\rho_f\, r^2\,\Omega^2\, A + \rho_f\, w_0^2\, P(\eta,\tau), \quad \eta = \frac{z\,\Omega}{w_0}. \end{aligned}\right\}. \tag{16}$$

Then, time-dependent derivatives are included in equations (2) to (5) for unsteady flow equations:

$$\frac{\partial u}{\partial t}+u\frac{\partial u}{\partial r}+w\frac{\partial u}{\partial z}-\frac{v^2}{r}=-\frac{1}{\rho_n}\frac{\partial p}{\partial r}+\frac{\mu_n}{\rho_n}\left[\left(\frac{\partial}{\partial r}\left(\frac{u}{r}\right)\right)+\frac{\partial^2 u}{\partial z^2}\right], \tag{17}$$

$$\frac{\partial v}{\partial t}+\frac{u}{r}\frac{\partial (r\,v)}{\partial r}+w\frac{\partial v}{\partial z}=\frac{\mu_n}{\rho_n}\left[\left(\frac{\partial}{\partial r}\left(\frac{v}{r}\right)\right)+\frac{\partial^2 v}{\partial z^2}\right], \tag{18}$$

$$\frac{\partial w}{\partial t}+u\frac{\partial w}{\partial r}+w\frac{\partial w}{\partial z}=-\frac{1}{\rho_n}\frac{\partial p}{\partial z}+\frac{\mu_n}{\rho_n}\left[\frac{1}{r}\frac{\partial w}{\partial r}+\frac{\partial^2 w}{\partial z^2}\right], \tag{19}$$

$$\frac{\partial T}{\partial t}+u\frac{\partial T}{\partial r}+w\frac{\partial T}{\partial z}=\frac{k_n}{(\rho\,C_p)_n}\left[\frac{1}{r}\frac{\partial T}{\partial r}+\frac{\partial^2 T}{\partial z^2}\right]-\frac{1}{(\rho\,C_p)_n}\frac{\partial q_r}{\partial z}+\frac{Q_0}{(\rho\,C_p)_n}(T-T_2). \tag{20}$$

After eliminating the pressure term in equations (17) and (19), we obtain the following:

$$\frac{\partial}{\partial z}\left(\frac{\partial u}{\partial t}\right)-\frac{\partial}{\partial r}\left(\frac{\partial w}{\partial t}\right)+\frac{\partial}{\partial z}\left(u\frac{\partial u}{\partial r}\right)+\frac{\partial}{\partial z}\left(w\frac{\partial u}{\partial z}\right)-\frac{\partial}{\partial r}\left(w\frac{\partial w}{\partial z}\right)-\frac{\partial}{\partial z}\left(\frac{v^2}{r}\right)$$
$$=\frac{\mu_n}{\rho_n}\left[\frac{\partial}{\partial z}\left(\frac{\partial}{\partial r}\left(\frac{u}{r}\right)\right)+\frac{\partial}{\partial z}\left(\frac{\partial^2 u}{\partial z^2}\right)-\frac{\partial}{\partial r}\left(\frac{\partial^2 w}{\partial z^2}\right)\right]. \tag{21}$$

The similarity variables (16) are substituted into equations (18), (20), and (21), which results:

$$\frac{1}{Re}\frac{\mu_n/\mu_f}{\rho_n/\rho_f}\frac{\partial^4 f}{\partial \eta^4}+2f\frac{\partial^3 f}{\partial \eta^3}+2g\frac{\partial g}{\partial \eta}-\frac{\partial^3 f}{\partial \eta^2\,\partial \tau}=0, \tag{22}$$

$$\frac{1}{Re}\frac{\mu_n/\mu_f}{\rho_n/\rho_f}\frac{\partial^2 g}{\partial \eta^2}+2f\frac{\partial g}{\partial \eta}-2g\frac{\partial f}{\partial \eta}-\frac{\partial g}{\partial \tau}=0, \tag{23}$$

$$\frac{1}{PrRe}\frac{1}{(\rho C_p)_n/(\rho C_p)_f}\left(\frac{k_n}{k_f}+\frac{4}{3}Rd\right)\frac{\partial^2 \theta}{\partial \eta^2}+2f\frac{\partial \theta}{\partial \eta}+\frac{Q\,\theta}{(\rho C_p)_n/(\rho C_p)_f}-\frac{\partial \theta}{\partial \tau}=0, \tag{24}$$

with the boundary conditions:

$$\left.\begin{aligned} f(0,\tau)=0,\ \frac{\partial f}{\partial \eta}(0,\tau)=0,\ g(0,\tau)=0,\quad \theta(0,\tau)=1,\\ \theta(1,\tau)=0,\ \frac{\partial f}{\partial \eta}(1,\tau)=0,\quad g(1,\tau)=\lambda,\quad f(1,\tau)=-\frac{\varepsilon}{2}. \end{aligned}\right\}. \tag{25}$$

Next, we consider the following perturbation function (Waini et al., 2022):

$$\begin{aligned} f(\eta,\tau)&=f_0(\eta)+e^{-\gamma\tau}F(\eta,\tau),\\ g(\eta,\tau)&=g_0(\eta)+e^{-\gamma\tau}G(\eta,\tau),\\ \theta(\eta,\tau)&=\theta_0(\eta)+e^{-\gamma\tau}H(\eta,\tau), \end{aligned} \tag{26}$$

with γ as the eigenvalue. The arbitrary functions $F(\eta,\tau)$, $G(\eta,\tau)$, and $H(\eta,\tau)$ and their derivatives are relatively smaller than $f_0(\eta)$, $g_0(\eta)$, and $\theta_0(\eta)$ and their derivatives. Equation (26) will be substituted into equations (22) to (25) to obtain the eigenvalue problem. Then, $F(\eta,\tau)=F_0(\eta)$, $G(\eta,\tau)=G_0(\eta)$, and $H(\eta,\tau)=H_0(\eta)$ when $\tau=0$ to determine the initial decay or growth of disturbance in the solutions (Weidman et al., 2006). Thus, the linearised eigenvalue problem is given by:

$$\frac{1}{Re}\frac{\mu_n/\mu_f}{\rho_n/\rho_f}F_0'''' + 2f_0F_0''' + 2F_0f_0''' + 2g_0G_0' + 2G_0g_0' + \gamma F_0'' = 0, \quad (27)$$

$$\frac{1}{Re}\frac{\mu_n/\mu_f}{\rho_n/\rho_f}G_0'' + 2f_0G_0' + 2F_0g_0' - 2g_0F_0' - 2G_0f_0' + \gamma G_0 = 0, \quad (28)$$

$$\frac{1}{PrRe}\frac{1}{(\rho C_p)_n/(\rho C_p)_f}\left(\frac{k_n}{k_f}+\frac{4}{3}Rd\right)H_0'' + 2f_0H_0' + 2F_0\theta_0' + \frac{Q}{(\rho C_p)_n/(\rho C_p)_f}H_0 + \gamma H_0 = 0, \quad (29)$$

along with the boundary conditions:

$$\left.\begin{aligned} F_0(0)=0,\ F_0'(0)=0,\ G_0(0)=0,\quad H_0(0)=0,\\ H_0(1)=0,\ F_0'(1)=0,\quad G_0(1)=0,\quad F_0(1)=0. \end{aligned}\right\}. \quad (30)$$

Here, the boundary condition $F_0'(1)=0$ is relaxed to form $F_0''(0)=1$ for the possible range of eigenvalues ($\gamma_1<\gamma_2<\gamma_3<\gamma_4<\cdots$) that will be computed using the bvp4c solver in MATLAB (Zainal et al., 2021). The smallest eigenvalue, γ_1, decides the solutions' stability, with a positive value referring to a physically meaningful and stable solution with decaying disturbance. In contrast, a negative value denotes an unstable solution with a growing disturbance that may promote boundary later separation.

RESULTS AND DISCUSSION

The numerical solution generated by the bvp4c solver is compared with the approximate solution obtained by Kavenuke et al. (2009). The previous study calculated the solution using the perturbation technique and Paté's approximation. The results from both studies show a good agreement, as shown in Fig. 2.

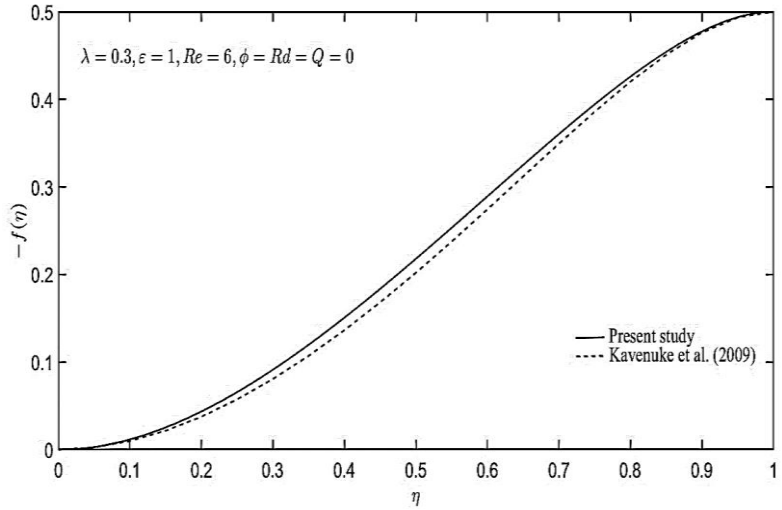

Figure 2. Comparison of the current $-f'(\eta)$ profile with the previous study.

The computation of boundary value problems (13) to (15) using the bvp4c solver in MATLAB produces dual solutions. In the following results, the solutions are termed the first and second solutions. These solutions are generated by different initial guesses made in the solver. Thus, it is crucial to determine the stability and significance of these solutions. Through stability analysis, we identify the first solution as the stable solution while the second solution is unstable. The values of γ_1 for the first and second solutions are tabulated in Table 2.

Table 2. Smallest eigenvalues for solutions of various nanofluids when $\phi = 0.2, \lambda = -1, \varepsilon = 1, Re = 9, Rd = 0.3$, and $Q = 0.1$

Nanofluid	γ_1	
	First solution	Second solution
$CoFe_2O_4/H_2O$	0.38353	-0.27080
$Mn\text{-}ZnFe_2O_4/H_2O$	0.37739	-0.27002
$CoFe_2O_4/C_2H_6O_2$	0.13611	-0.19540
$Mn\text{-}ZnFe_2O_4/C_2H_6O_2$	0.13639	-0.19420

The effects of nanoparticle volume fraction on the nanofluid flow and thermal fields are depicted in Fig. 3. The increase in ϕ enhances the radial and tangential velocities near the lower and upper disks. However, the axial velocity near the rotating upper disk reduces with the increment of ϕ, as shown by the profile in Figure 3a. In Figure 3d, it can be noticed that the increase in ϕ has different effects on the temperature profile of the water-based nanofluids and ethylene glycol-based nanofluids. The temperature profiles of the ethylene glycol-based nanofluids rise with ϕ, but the opposite is obtained for the water-based nanofluids.

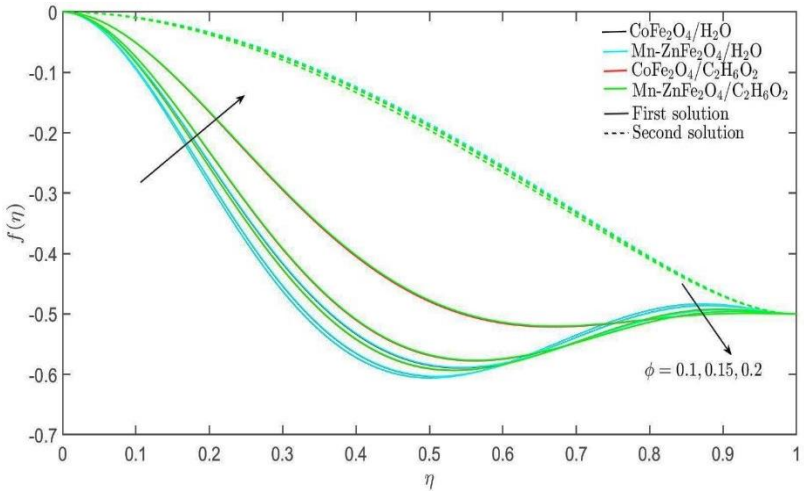

(a)

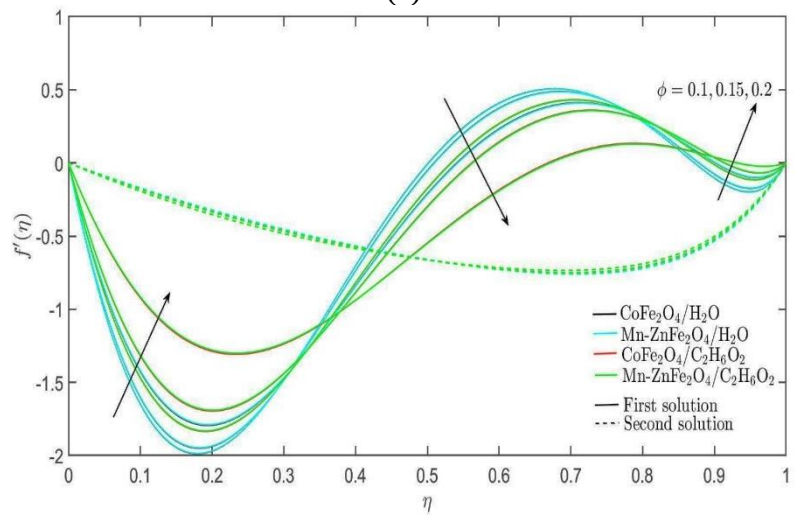

(b)

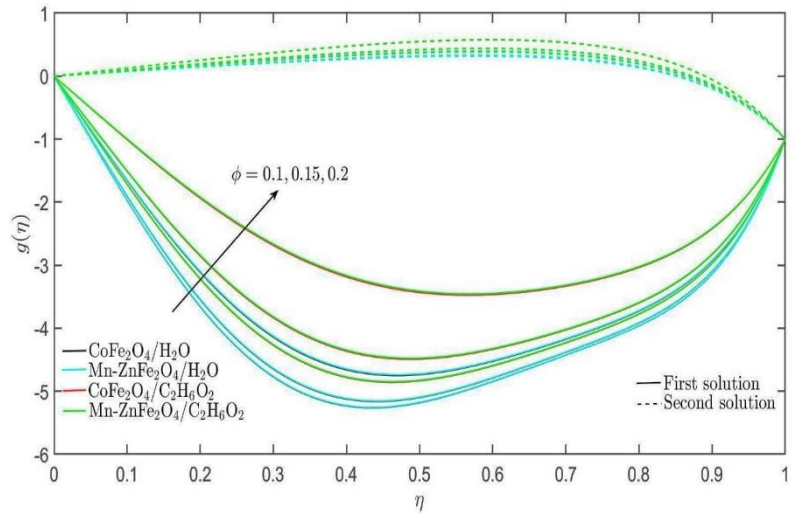

(c)

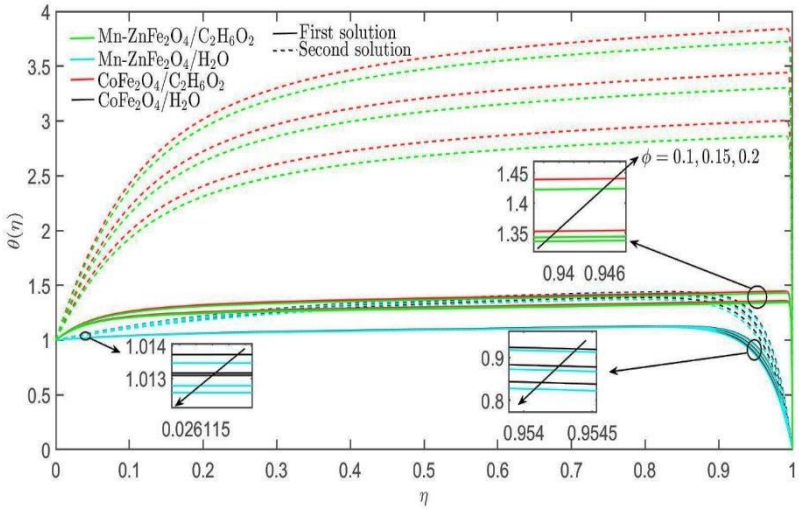

(d)

Figure 3. Profiles of (a) axial velocity, (b) radial velocity, (c) tangential velocity, and (d) temperature with different nanoparticle volume fractions when $\lambda = -1, \varepsilon = 1, Re = 9, Rd = 0.3$, and $Q = 0.1$.

Figure 4 portrays the impacts of shrinking parameter on the profiles of the nanofluid's temperature and axial, radial, and tangential velocities. As presented in Figs. 4a and 4c, the augmentation of $|\lambda|$ reduce the axial and tangential velocities of the internal flow between the disks. However, the increase in $|\lambda|$ affects the radial velocity differently in the region near the lower disk, between the disks, and the upper disk, as shown in Fig. 4b. The $f'(\eta)$ profile near the lower disk decreases with $|\lambda|$. Away from the non-permeable lower disk, the radial velocity profile improves with $|\lambda|$. In contrast, a decreasing behaviour is seen in the region near the permeable upper disk for the radial velocity profiles of the water-based nanofluids. Meanwhile, the temperature profiles of water- and ethylene glycol-based nanofluids in Fig. 4d diminish with the increase in the magnitude of the shrinking parameter.

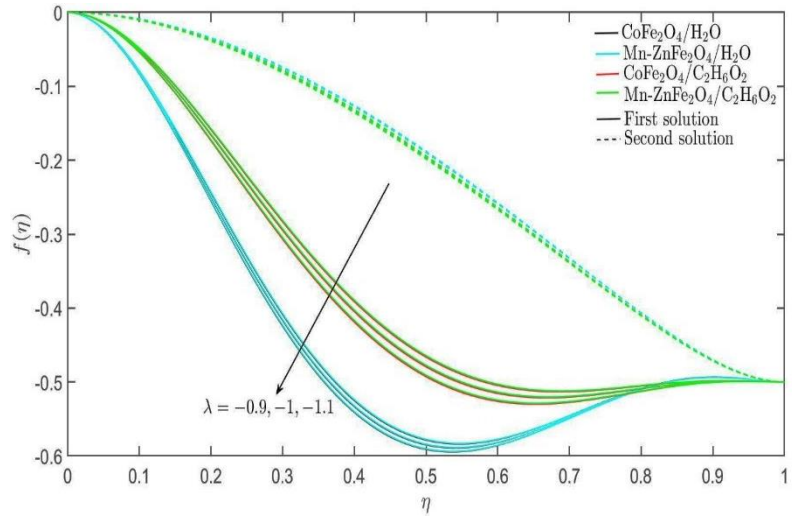
$CoFe_2O_4/H_2O$
$Mn\text{-}ZnFe_2O_4/H_2O$
$CoFe_2O_4/C_2H_6O_2$
$Mn\text{-}ZnFe_2O_4/C_2H_6O_2$
First solution
Second solution
$\lambda = -0.9, -1, -1.1$
$f(\eta)$
η

(a)

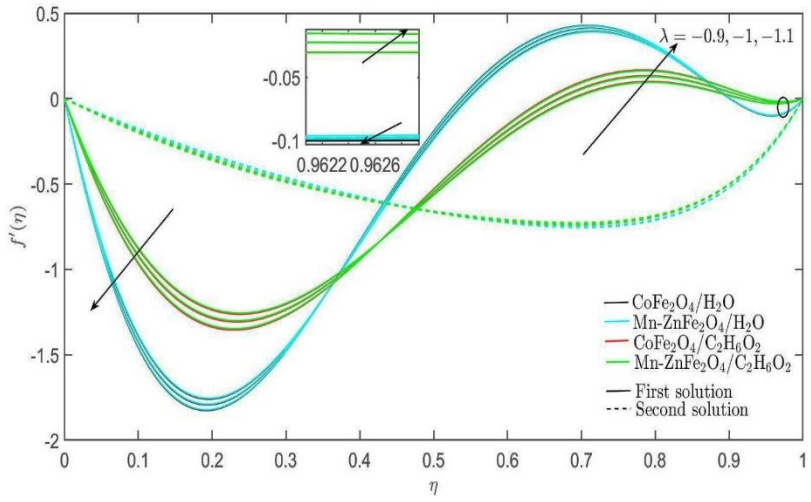
$\lambda = -0.9, -1, -1.1$
-0.05
-0.1
0.9622 0.9626
$f'(\eta)$
$CoFe_2O_4/H_2O$
$Mn\text{-}ZnFe_2O_4/H_2O$
$CoFe_2O_4/C_2H_6O_2$
$Mn\text{-}ZnFe_2O_4/C_2H_6O_2$
First solution
Second solution
η

(b)

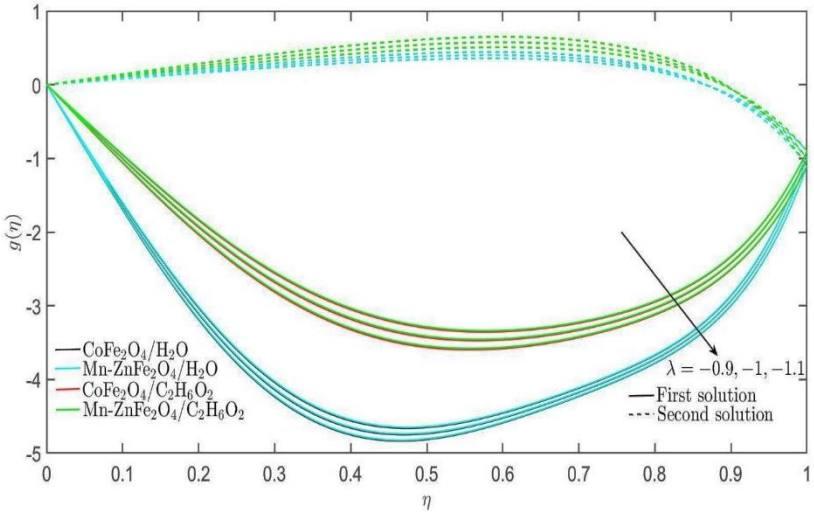
$g(\eta)$
$CoFe_2O_4/H_2O$
$Mn\text{-}ZnFe_2O_4/H_2O$
$CoFe_2O_4/C_2H_6O_2$
$Mn\text{-}ZnFe_2O_4/C_2H_6O_2$
$\lambda = -0.9, -1, -1.1$
First solution
Second solution
η

(c)

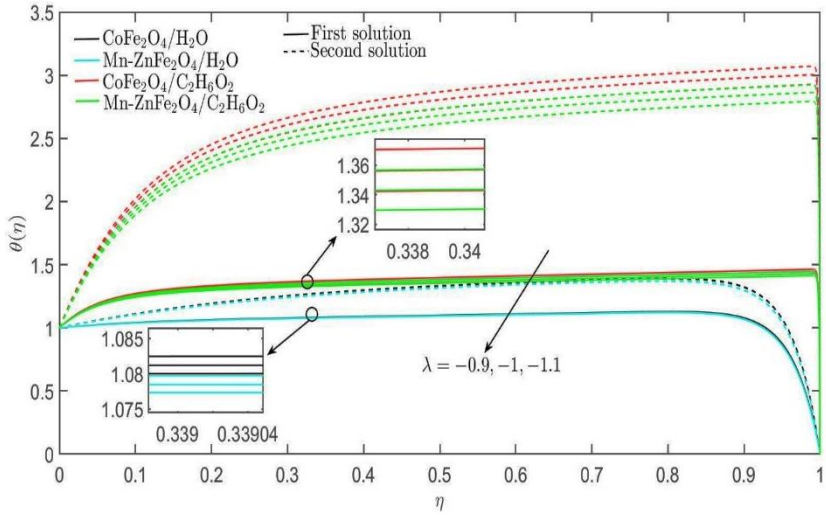

(d)

Figure 4. Profiles of (a) axial velocity, (b) radial velocity, (c) tangential velocity, and (d) temperature with different values of the shrinking parameter when $\phi = 0.2, \varepsilon = 1, Re = 9, Rd = 0.3$, and $Q = 0.1$.

Then, the velocities and temperature profiles with various values of Reynolds number are depicted in Fig. 5. The axial velocity profile in Fig. 5a shows a reducing trend for the region near the stationary lower disk as the value of Re increases. However, the axial velocity profile rises when approaching the rotating upper disk. In contrast, the radial velocity profile at the region near the disks diminishes as Re increases, as shown in Fig. 5b. Meanwhile, the tangential velocity profile throughout the internal flow reduces as Re increases. Similar behaviour is observed for the temperature profile in Fig. 5d, except around the upper disk. The temperature profiles for the water-based nanofluids show an increasing trend with Re near the upper disk. Since $Re = \frac{w_0^2}{\Omega \nu_f}$, the increase in Re denotes the enhancement of suction and the reduction of kinematic viscosity and angular velocity. Consequently, it induces the declination of the velocity profile, as obtained in Fig. 5c. In addition, suction allows heated fluid to be removed from the permeable surface, which leaves behind cold fluid that causes the temperature profile to drop (Ajibade et al., 2021). Thus, this explains the results generated in Fig. 5d with the increasing values of Re.

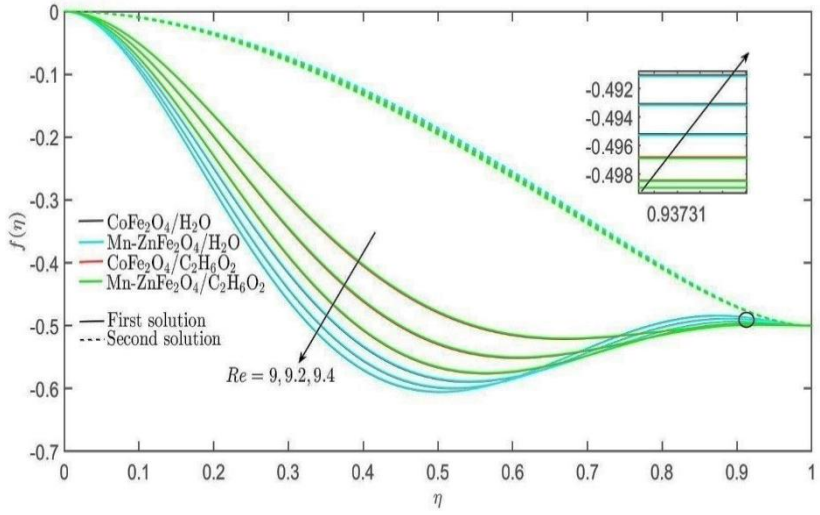

(a)

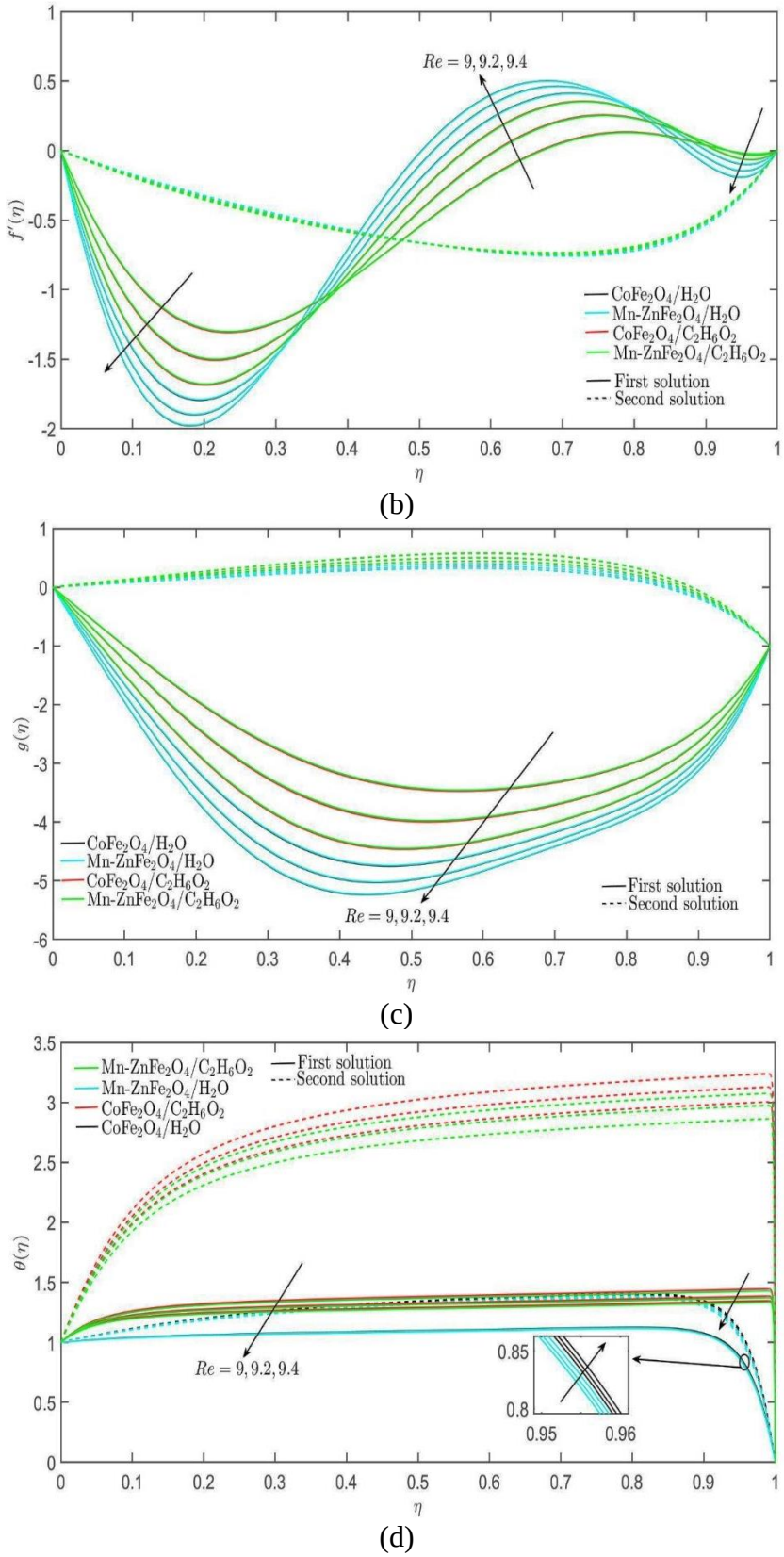

Figure 5. Profiles of (a) axial velocity, (b) radial velocity, (c) tangential velocity, and (d) temperature with different values of Reynolds number when $\phi = 0.2, \varepsilon = 1, \lambda = -1, Rd = 0.3,$ and $Q = 0.1$.

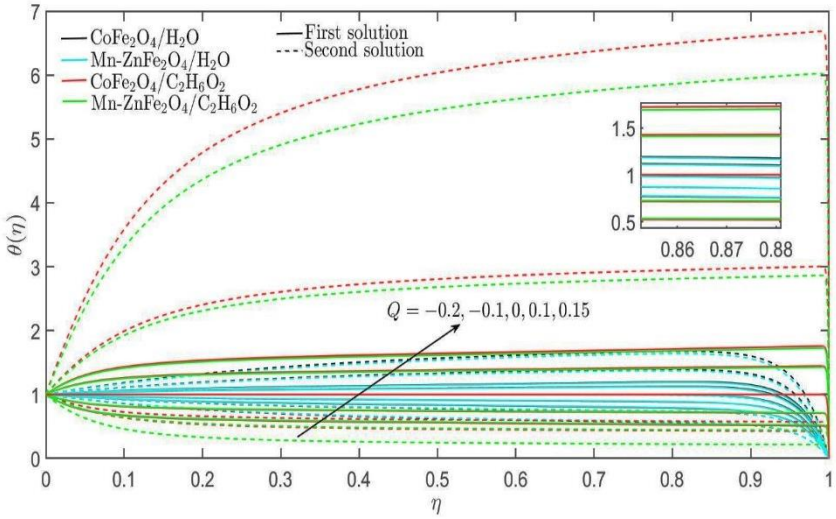

Figure 6. Profiles of temperature with different values of heat generation/absorption parameter when $\phi = 0.2, \varepsilon = 1, \lambda = -1, Rd = 0.3$, and $Re = 9$.

Meanwhile, the negative value of Q represents heat absorption, while the positive value implies heat generation. An additional heat source in the system due to the increased heat generation parameter promotes the increase of the temperature profile, as obtained in Fig. 6. Similar behaviour was recorded by Upadhya et al. (2021) and Bilal et al. (2022).

In contrast, the presence of the thermal radiation parameter reduces the temperature profile, as shown in Fig. 7. As Bilal et al. (2022) explained, the increase in radiation from the fluid surface cools down the fluid and causes the temperature profile to drop.

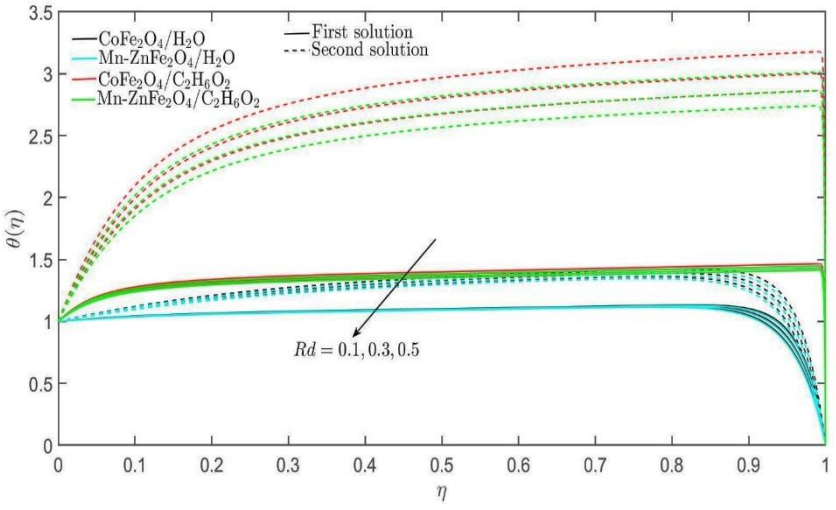

Figure 7. Profiles of temperature with different values of radiation parameter when $\phi = 0.2, \varepsilon = 1, \lambda = -1, Q = 0.1$, and $Re = 9$.

CONCLUSION

In the present study, the internal flow of nanofluid between disks is analysed. The working fluid consisting of different combinations of nanoparticles and base fluid (i.e., $CoFe_2O_4/H_2O$, $Mn\text{-}ZnFe_2O_4/H_2O$, $CoFe_2O_4/C_2H_6O_2$, and $Mn\text{-}ZnFe_2O_4/C_2H_6O_2$) are considered in this flow problem. Partial differential equations and boundary conditions governing the flow problem are

incorporated with thermal radiation and heat generation effects. Then, similarity transformations are utilised for deriving the non-linear ordinary differential equations and boundary conditions for numerical computation in MATLAB. The computation obtained dual solutions, and the stability analysis confirmed that only the first solution is stable. Other findings can be summarised as follows:

1. The temperature profile of the ethylene-glycol-based nanofluids (i.e., $CoFe_2O_4/C_2H_6O_2$ and $Mn\text{-}ZnFe_2O_4/C_2H_6O_2$) rises with the addition of nanoparticle volume fraction, contrary to the water-based nanofluids (i.e., $CoFe_2O_4/H_2O$ and $Mn\text{-}ZnFe_2O_4/H_2O$).
2. The profiles of axial and tangential velocities diminish with the increase in the shrinking parameter.
3. The increase in Reynolds number reduces the tangential velocity profile of the nanofluid.
4. The augmentation of the heat generation and radiation parameters elevates and reduces the temperature profile, respectively.

REFERENCES

Ahmadian, A., Bilal, M., Khan, M. A. and Asjad, M. I. (2020), The non-Newtonian maxwell nanofluid flow between two parallel rotating disks under the effects of magnetic field, *Sci. Rep.*, **10(1)**: 17088. https://doi.org/10.1038/s41598-020-74096-8

Ahmed. N., Tassaddiq, A., Alabdan, R., Khan, U., Noor, S., Mohyud-Din, S. T. and Khan, I. (2019), Applications of nanofluids for the thermal enhancement in radiative and dissipative flow over a wedge, *Appl. Sci.*, **9(10)**: 1976. https://doi.org/10.3390/app9101976

Ajibade, A. O., Umar, A. M. and Kabir, T. M. (2021), An analytical study on effects of viscous dissipation and suction/injection on a steady mhd natural convection couette flow of heat generating/absorbing fluid, *Adv. Mech. Eng.*, **13(5)**: 16878140211015862. https://doi.org/10.1177/16878140211015862

Awati, V. B., Makinde, O. D. and Jyoti, M. (2018), Computer-extended series solution for laminar flow between a fixed impermeable disk and a porous rotating disk, *Eng. Comput.*, **35(4)**: 1655 – 1674. https://doi.org/10.1108/EC-01-2017-0021

Bataller, R. C. (2008), Radiation effects for the Blasius and Sakiadis flows with a convective surface boundary condition, *Appl. Math. Comput.*, **206(2)**: 832 – 840. https://doi.org/10.1016/j.amc.2008.10.001

Bilal, M., Ayed, H., Saeed, A., Brahmia, A., Gul, T. and Kumam, P. (2022), The parametric computation of non-linear convection magnetohydrodynamic nanofluid flow with internal heating across a fixed and spinning disk, *Waves in Random and Complex Media*, 1 – 16. https://doi.org/10.1080/17455030.2022.2042621

Duguma, K. A., Makinde, O. D. and Enyadene, L. G. (2023), Stability analysis of dual solutions of convective flow of casson nanofluid past a shrinking/stretching slippery sheet with thermophoresis and brownian motion in porous media, *J. Math.* **2023**. https://doi.org/10.1155/2023/5954860

Ghasemi, S. E., and Gouran, S. (2023), Mathematical simulation of laminar micropolar fluid flow between two disks for two different geometries, *Waves in Random and Complex Media*, 1 – 22. https://doi.org/10.1080/17455030.2023.2182139

Habu, P. N., Al'aidrus, S. N., Mohd Noor, N. F. and Siri, Z. (2022), Mass transfer of a thermally radiative mhd cattaneo-christov nanofluid between two stretchable spinning disks, *Sains Malaysiana*, **51(7)**: 2223 – 2235. http://doi.org/10.17576/jsm-2022-5107-23

Hussain, T. and Xu, H. (2022), Time-dependent squeezing bio-thermal MHD convection flow of a micropolar nanofluid between two parallel disks with multiple slip effects, *Case Stud. Therm. Eng.*, **31**: 101850. https://doi.org/10.1016/j.csite.2022.101850

Ishak, A. (2010), Thermal boundary layer flow over a stretching sheet in a micropolar fluid with

radiation effect, *Meccanica*, **45**: 367-373. https://doi.org/10.1007/s11012-009-9257-4

Jalili, B., Roshani, H., Jalili, P., Jalili, M., Pasha, P. and Ganji, D. D. (2023), The magnetohydrodynamic flow of viscous fluid and heat transfer examination between permeable disks by AGM and FEM, *Case Stud. Therm. Eng.*, **45**: 102961. https://doi.org/10.1016/j.csite.2023.102961

Kavenuke D. P., Massawe E. and Makinde O. D. (2009), Modeling laminar flow between a fixed impermeable disk and a porous rotating disk, *Afr. J. Math. Comput. Sci. Res.*, **2**: 157 – 162.

Khan, M. I., Alzahrani, F. and Hobiny, A. (2023), Mathematical modeling and heat transfer in nanofluid flow of Newtonian material between two rotating disks, *Appl. Nanosci.*, 13(1): 201 – 212. https://doi.org/10.1007/s13204-020-01586-6

Khan, N. and Mahmood, T. (2016), Thermophoresis particle deposition and internal heat generation on MHD flow of an Oldroyd-B nanofluid between radiative stretching disks, *J. Mol. Liq.*, **216**: 571 – 582. https://doi.org/10.1016/j.molliq.2016.01.074

Kilic, M. and Owen, J. M. (2003), Computation of flow between two disks rotating at different speeds, *J. Turbomach.*, **125(2)**: 394 – 400. https://doi.org/10.1115/1.1539515

Lanjwani, H. B., Anwar, M. I., Ghoto, A. A., Shehzad, S. A. and Zaimi, M. K. (2023), Stability analysis and dual solutions of time-dependent stagnation-point heat transport of Casson nanofluid by using Tiwari–Das model, *Numer. Heat Transf B: Fundam.*, 1 – 18. https://doi.org/10.1080/10407790.2023.2200214

Magyari, E. and Pantokratoras, A. (2011), Note on the effect of thermal radiation in the linearized Rosseland approximation on the heat transfer characteristics of various boundary layer flows, *Int. Commun. Heat Mass Transf.*, **38(5)**: 554 – 556. https://doi.org/10.1016/j.icheatmasstransfer.2011.03.006

Merkin, J. H. (1986), On dual solutions occurring in mixed convection in a porous medium, *J. Eng. Math.*, **20(2)**: 171 – 179. https://doi.org/10.1007/BF00042775

Rajagopal, K. R. (1992), Flow of viscoelastic fluids between rotating disks, *Theor. Comput. Fluid Dyn.*, **3(4)**: 185 – 206. https://doi.org/10.1007/BF00417912

Soong, C. Y. (2003), Flow structure and heat transfer between two disks rotating independently, *J. Therm. Sci.*, **12**: 62 – 76. https://doi.org/10.1007/s11630-003-0011-2

Umavathi, J. C., Prakasha, D. G., Alanazi, Y. M., Lashin, M. M. A., Al-Mubaddel, F. S., Kumar, R. and Gowda, R. J. P. (2023), Magnetohydrodynamic squeezing Casson nanofluid flow between parallel convectively heated disks, *Int. J. Mod. Phys. B*, **37(4)**: 2350031. https://doi.org/10.1142/S0217979223500315

Upadhya, S. M., Renuka Devi, R. L. V., Raju, C. S. K. and Muhammad Ali, H. (2021), Magnetohydrodynamic non-linear thermal convection nanofluid flow over a radiated porous rotating disk with internal heating, *J. Therm. Anal. Calorim.*, **143**: 1973 – 1984. https://doi.org/10.1007/s10973-020-09669-w

Usman, A. G., Muhammad, T. and Mustafa, I. (2022), Heat transfer enhancement in a power-law nanofluid flow between two rotating stretchable disks, *Pramana*, **96(1)**: 40. https://doi.org/10.1007/s12043-021-02272-0

Waini, I., Khashi'ie, N. S., Mohd Kasim, A. R., Zainal, N. A., Ishak, A. and Pop, I. (2022), Radiative heat transfer of Reiner–Philippoff fluid flow past a nonlinearly shrinking sheet: Dual solutions and stability analysis, *Chin. J. Phys.*, **77**: 45 – 56. https://doi.org/10.1016/j.cjph.2021.11.037

Wehgal, A. R. and Ashraf, M. (2020), MHD asymmetric flow between two porous disks, *Punjab Univ. J. Math.*, **44(1)**.

Weidman, P. D., Kubitschek, D. G. and Davis, A. M. J. (2006), The effect of transpiration on self-similar boundary layer flow over moving surfaces, *Int. J. Eng. Sci.*, **44(11-12)**: 730 – 737. https://doi.org/10.1016/j.ijengsci.2006.04.005

Yahaya, R. I., Arifin, N. M., Ali, F. M. and Mohamed Isa, S. S. P. (2023), Nanofluid flow and heat

transfer between a stationary non-permeable disk and a permeable rotating shrinking disk with radiation and heat generation effects, *J. Adv. Res. Fluid Mech. Therm. Sci.*, **101(1)**: 37 – 44. https://doi.org/10.37934/arfmts.101.1.3744

Zainal, N. A., Nazar, R., Naganthran, K. and Pop, I. (2021), Stability analysis of MHD hybrid nanofluid flow over a stretching/shrinking sheet with quadratic velocity, *Alex. Eng. J.*, **60(1)**: 915 – 926. https://doi.org/10.1016/j.aej.2020.10.020

Zulkifli, A. M. and Md Ali, F. (2023), Wang's stretching/shrinking sheet problem for nanofluids with the effects of suction and injection, *Menemui Matematik (Discovering Mathematics)*, **45(1)**: 12 – 20. https://myjms.mohe.gov.my/index.php/dismath/article/view/22869